INTERNATIONAL JOURNAL FOR NUMERICAL METHODS IN FLUIDS
Int. J. Numer. Meth. Fluids **31**: 1195–1220 (1999)

DISCRETE FILTERS FOR LARGE EDDY SIMULATION

P. SAGAUT* AND R. GROHENS

ONERA, 29 avenue de la Division Leclerc, 92322 Châtillon Cedex, France

SUMMARY

This paper summarizes several results relative to discrete filters for subgrid-scale (SGS) models based on a multi-level filtering procedure. First, a theoretical study of discrete filters in physical space is performed. The analysis is done in the uniform one-dimensional case, and is then extended to the general multi-dimensional case for arbitrary structured and unstructured meshes. Some equivalence classes for the discrete filters are defined, based either on a differential approximation or the associated transfer function. Methods for the definition of discrete filters are proposed in the general case, including the approximation of continuous convolution filters. Second, the sensitivity of several SGS models with respect to the test filter is investigated. The selected models are: the dynamic Smagorinsky model, the mixed scale model (MSM), the selective MSM and the Liu–Meneveau–Katz (LMK) similarity model. Improved versions, which explicitly account for the spectral width of the test filter of the MSM and the LMK similarity model are proposed. The analysis, which reveals a significant influence of the test filter, is done through *a priori* testing on a 128^3 field issued from the large eddy simulation (LES) of freely decaying homogeneous isotropic turbulence. Copyright © 1999 John Wiley & Sons, Ltd.

KEY WORDS: large eddy simulation; subgrid-scale model; filter

1. INTRODUCTION

Large eddy simulation (LES) [1,2] is a promising technique for the unsteady calculation of complex flows. It is based on the decomposition of the flow in low-frequency resolved modes and high-frequency unresolved modes (*subgrid-scale modes*), the latter being parametrized through the use of a *subgrid-scale* (SGS) *model*. This scale separation is achieved by applying a filter, hereafter referred to as the *LES filter*, to the Navier–Stokes equation.

The SGS models must represent the unresolved modes on the basis of the information contained in the simulation, i.e. the resolved modes. Various SGS models have been proposed and it appears that the most efficient ones are based on the analysis of the resolved modes of highest frequency. These modes, which constitute the *test field*, are extracted from the resolved field through the application of a low-pass filter, referred to as the *test filter*.

Examples are the turbulent kinetic energy (TKE) model by Bardina *et al.* [3], which links the amplitude of the model to the kinetic energy of the test field, and the mixed scale model (MSM) by Sagaut and Loc (see Reference [4] for a description), which is a generalization of the TKE and Smagorinsky [5] models. Some improved versions of the original structure function model of Métais and Lesieur [6] have recently been proposed, which involve the test

* Correspondence to: ONERA, DSNA/ETRI, 29 avenue de la Division Leclerc, 92322 Chatillon Cedex, France. E-mail: sagaut@onera.fr

CCC 0271–2091/99/241195–26$17.50

Received 13 October 1997
Revised 4 August 1998

field: the selective structure function model [7], which includes a test on the topology of the vorticity of the test field, and the filtered structure function model [7,8], which evaluates the model on the test field. At last, the Germano–Lilly dynamic procedure [9,10], based on the Germano relationship which links without any approximation of the SGS tensors associated with different levels of filtering, including its numerous variants [11,12], is now very popular.

Other SGS models, based on the scale similarity hypothesis of Bardina *et al.* [3], also rely on a mutli-filtering approach. The original model, which involves several applications of the same filter (i.e. the LES filter and the test filter are identical), has recently been generalized by Liu *et al.* [13] in the case of different cut-off wavenumbers for the two filtering levels, and to the use of different filters by Shah and Ferziger [14].

Whereas the strong influence of the nature of the LES filter on the interactions between resolved and subgrid-scales has been demonstrated by theoretical analysis [15] and numerical experiments [16], the dependency of multi-level SGS models on the test filter remains to be investigated. Germano *et al.* [9] indicate that, for the dynamic Smagorinsky model, the optimal ratio between the cut-off length-scale of the LES filter and the test filter is 2. Najjar and Tafti [17] recently investigated the dependency of the dynamic procedure on the discrete form of the test filter used during the simulation, and have demonstrated a strong dependency of the results, the best results being obtained with the most local wavenumber filters.

Now the problem of the definition of discrete test filters suitable for simulations of industrial interest appears. Theoretical studies on SGS modelling were carried out considering filtering operations that are defined as convolution products between the velocity field and the filter kernel. That definition is suitable when dealing with numerical methods such as spectral or pseudo-spectral methods, but is very expensive when dealing with local methods (finite differences, finite volumes, finite elements). In practice, for local methods, discrete test filters with compact stencils based on weighted averages are used. For example, in the uniform one-dimensional case, most of the authors consider the two following three-point filters:

$$\bar{\phi}_i = \frac{1}{4}(\phi_{i-1} + 2\phi_i + \phi_{i+1}) \quad \text{or} \quad \bar{\phi}_i = \frac{1}{6}(\phi_{i-1} + 4\phi_i + \phi_{i+1}).$$

These two filters are obtained by applying respectively the trapezoidal rule and the Simpson rule to compute the average of the variable ϕ over the control cell surrounding the point i.

The properties of these discrete filters differ a lot from those of the continuous filters, which are the basis of theoretical analysis. Hence, the need for the analysis of discrete filters, and for the definition of discrete filters with required properties in order to ensure a greater consistency between the continuous SGS model and its discretized version, which will be used for the computation, appears.

The present paper summarizes results relative to discrete filters for LES, and presents a general framework for their analysis and classification. It is organized as follows. Section 2 details the general analysis of discrete filters in the uniform one-dimensional case. Associated continuous differential operators and transfer functions are derived and equivalence classes for discrete filters are proposed. Two ways of extending it to the multi-dimensional case are given in Section 3, while the generalization to curvilinear and unstructured meshes is proposed in Section 4. Several discrete approximation methods for continuous convolution filters are examined in Section 5. Section 6 is dedicated to the definition of discrete bandpass-like filters. The dependency of several SGS models on the discrete test filter is investigated in Section 7 through some *a priori* tests performed on isotropic homogeneous turbulence. Some improved models are proposed, which account explicitly for the test filter. Conclusions are presented in Section 8.

2. DISCRETE FILTERS IN THE UNIFORM ONE-DIMENSIONAL CASE

2.1. Discrete operator and associated transfer function

The filtered field at the ith grid point $\bar{\phi}_i$, obtained by applying a discrete $(2N+1)$-point filter F to the variable ϕ, is formally defined as

$$\bar{\phi}_i = F\phi_i \equiv \sum_{l=-N}^{N} a_l \phi_{i+l}, \tag{1}$$

where the real coefficients a_k specify the filter. The preservation of a constant variable is ensured under the condition

$$\sum_{l=-N}^{N} a_l = 1.$$

The spectral signature of the discrete filter F defined by Equation (1) is characterized by the associated transfer function $\hat{F}$, which is computed via a von Neumann analysis. Considering monochromatic waves of the form $\phi(\xi) = \mathrm{e}^{\mathrm{j}k\xi}$, with $\mathrm{j}^2 = -1$, and assuming that the grid is uniform ($\Delta\xi_n \equiv \xi_{n+1} - \xi_n = \Delta\xi$), the associated transfer function is

$$\hat{F}(k) = \sum_{l=-N}^{N} a_l \, \mathrm{e}^{\mathrm{j}kl\Delta\xi}. \tag{2}$$

Its real part $\hat{F}_{\mathrm{Re}}(k)$ and the imaginary part $\hat{F}_{\mathrm{Im}}(k)$ are

$$\hat{F}_{\mathrm{Re}}(k) = \sum_{l=-N}^{N} a_l \cos(kl\Delta\xi), \qquad \hat{F}_{\mathrm{Im}}(k) = \sum_{l=-N}^{N} a_l \sin(kl\Delta\xi). \tag{3}$$

2.2. Equivalent continuous differential operator

The filtering operation associated with the application of the discrete filter (1) can be interpreted as the application of a differential operator to the continuous field ϕ. Assuming that the mesh is uniform and that the field ϕ is regular enough, one can introduce the Taylor series

$$\phi_{i\pm n} = \sum_{l=0}^{\infty} \frac{(\pm n\Delta\xi)^l}{l!} \left(\frac{\partial^l \phi}{\partial x^l}\right)_i. \tag{4}$$

Substituting that development into relation (1), one obtains

$$\bar{\phi}_i = \sum_{n=-N}^{N} a_n \sum_{l=0}^{\infty} \frac{(n\Delta\xi)^l}{l!} \left(\frac{\partial^l \phi}{\partial x^l}\right)_i. \tag{5}$$

This relation can be written as

$$\bar{\phi}_i = \sum_{l=0}^{\infty} a_l^* \Delta\xi^l \left(\frac{\partial^l \phi}{\partial x^l}\right)_i = \left(1 + \sum_{l=1}^{\infty} a_l^* \Delta\xi^l \frac{\partial^l}{\partial x^l}\right)\phi_i, \tag{6}$$

where the coefficients a_l^* are defined as

$$a_l^* = \frac{1}{l!} \sum_{n=-N}^{N} a_n n^l. \tag{7}$$

2.3. Equivalence classes for discrete filters

Discrete filters can be classified using some equivalence classes, which are arbitrarily defined. Two classes are proposed in this section: the first one is based on the transfer function concept, while the second one relies on the equivalent differential operator.

Definition 1
Two filters F and G are equivalent for wavenumber k_* if $\hat{F}(k_*) = \hat{G}(k_*)$.

Definition 2
Two filters F and G are equivalent to the nth order if $a_l^* = b_l^*$, $\forall l \in [0, \ldots, n]$, where the coefficients $\{a_l^*\}$ (respectively $\{b_l^*\}$) specify the continuous differential operator associated with F (respectively G).

3. EXTENSION TO THE MULTI-DIMENSIONAL CASE

For the sake of simplicity, the demonstration will be restricted to the case of the construction of a multi-dimensional filter on the basis of a unique one-dimensional filter, without any loss of generality.

A multi-dimensional filter F^p (where p is the dimension of space) can be constructed from a one-dimensional filter F in two different ways.

3.1. Construction by linear combination

The first method consists in operating a *linear combination of one-dimensional filters*, each direction of space being filtered independently of the others. This can be formally written as

$$F^p = \frac{1}{p} \sum_{i=1}^{p} F^i, \tag{8}$$

where F^i is the one-dimensional filter defined in the ith space direction. This linear combination can be interpreted as a simultaneous use of each one-dimensional filter. The stencil of the resulting discrete p-dimensional filter is the sum of each one-dimensional stencil, and then contains $(2pN+1)$ points for a $(2N+1)$-point one-dimensional filter. In the three-dimensional case, the filtered quantity becomes

$$\bar{\phi}_{i,j,k} = F^p \phi_{i,j,k} = \sum_{l=-N}^{N} a_l (\phi_{i+l,j,k} + \phi_{i,j+l,k} + \phi_{i,j,k+l}). \tag{9}$$

The associated transfer function is

$$\hat{F}^p(k_1, k_2, k_3) = \frac{1}{3} \sum_{l=-N}^{N} a_l (e^{jk_1 l\Delta\xi} + e^{jk_2\Delta\xi} + e^{jk_3\Delta\xi}). \tag{10}$$

The equivalent differential operator reads

$$\bar{\phi}_{i,j,k} = \left(1 + \sum_{l=1}^{\infty} \frac{a_l^*}{3} \Delta\xi^l \left[\frac{\partial^l}{\partial x_1^l} + \frac{\partial^l}{\partial x_2^l} + \frac{\partial^l}{\partial x_3^l}\right]\right) \phi_{i,j,k}. \tag{11}$$

3.2. Construction by product

The second method consists of defining the multi-dimensional filter F^p as the *composition of some one-dimensional filters* applied in each space direction. This can be formalized as follows:

$$F^p = \prod_{i=1}^{p} F^i. \tag{12}$$

This product is equivalent to a sequential application of the one-dimensional filter, and not to a simultaneous one as in the previous case. The resulting discrete filter has a $(2N+1)^3$-point stencil. In the three-dimensional case, the discrete operator reads

$$\bar{\phi}_{i,j,k} = F^p \phi_{i,j,k} = \sum_{l=-N}^{N} \sum_{m=-N}^{N} \sum_{n=-N}^{N} a_l a_m a_n \phi_{i+l,j+m,k+n}. \tag{13}$$

The associated transfer function is

$$\hat{F}^p(k_1, k_2, k_3) = \sum_{l=-N}^{N} \sum_{m=-N}^{N} \sum_{n=-N}^{N} a_l a_m a_n \, \mathrm{e}^{\mathrm{j}\Delta\xi(k_1 l + k_2 m + k_3 n)}. \tag{14}$$

The corresponding continuous differential operator has the form

$$\bar{\phi}_{i,j,k} = \prod_{i=1}^{3} \left(1 + \sum_{l=1}^{\infty} a_l^* \Delta\xi^l \frac{\partial^l}{\partial x_i^l} \right) \phi_{i,j,k}. \tag{15}$$

It should be noted that the multi-dimensional filters built up using these two methods with the same one-dimensional filter are not equivalent *a priori* for an arbitrary order $n \neq 0$ or a wavenumber $(k_1, k_2, k_3) \neq (0, 0, 0)$.

4. EXTENSION TO ARBITRARY MESH

The previous developments are valid for uniform Cartesian meshes. Several ways to extend the discrete filters on curvilinear structured and unstructured meshes can be considered. Two methods are proposed in this section, both of which rely on the equivalence classes defined previously.

The first solution consists of defining a continuous differential operator equivalent up to a chosen order n to the target filter. This technique is tractable for all mesh topologies, either structured or unstructured. It only necessitates the definition of the discrete differential operators that appear in the developments on the computational mesh. As discrete differential operators are already available in Navier–Stokes solvers, this approach leads to an immediate approximation of filters. This approach does not enforce the equivalence of the effective transfer functions because of the discretization errors appearing in the definition of the elementary discrete differential operators. Jansen [18] proposed a similar solution limited to the equivalence up to second order on unstructured meshes.

The second solution generates a discrete operator using m points, whose transfer function will be equivalent for a wavenumber $k^* = (k_1^*, k_2^*, k_3^*)$ to the one of the target filter. In order to define such an operator for a point of co-ordinates (x_0, y_0, z_0), using m points of co-ordinates $(x_l, y_l, z_l)_{1 \leq l \leq m}$, it is necessary to find the values of the weighting coefficients $\{a_l\}_{0 \leq l \leq m}$ that appear in the linear combination

$$\bar{\phi}(x_0, y_0, z_0) = \sum_{l=0}^{m} a_l \phi(x_l, y_l, z_l).$$

Defining the relative position of the lth point in the Cartesian basis centered on (x_0, y_0, z_0) as $(\Delta x_l = x_l - x_0, \Delta y_l = y_l - y_0, \Delta z_l = z_l - z_0)$, the real and imaginary parts of the transfer function can be written in the following forms:

$$\hat{F}_{\mathrm{Re}}(k_1, k_2, k_3) = a_0 + \sum_{l=1}^{m} a_l c_l, \qquad \hat{F}_{\mathrm{Im}}(k_1, k_2, k_3) = \sum_{l=1}^{m} a_l s_l. \tag{16}$$

The parameters $\{c_l\}$ and $\{s_l\}$ are defined as

$$c_l = \cos(k_1 \Delta x_l + k_2 \Delta y_l + k_3 \Delta z_l), \qquad s_l = \sin(k_1 \Delta x_l + k_2 \Delta y_l + k_3 \Delta z_l).$$

The coefficients $\{a_l\}$ are computed by solving the following linear system:

$$\begin{cases} a_0 + \sum_{l=1}^{m} a_l c_l = f_1(k_1^*, k_2^*, k_3^*), \\ \sum_{l=1}^{m} a_l s_l = f_2(k_1^*, k_2^*, k_3^*), \end{cases} \tag{17}$$

where $f_1(k_1^*, k_2^*, k_3^*)$ and $f_2(k_1^*, k_2^*, k_3^*)$ are arbitrarily fixed. Such a method allows the definition of a set of coefficients enforcing the equivalence simultaneously for at most $m/2$ different wavenumbers.

5. DISCRETE APPROXIMATION OF CONVOLUTION FILTERS

5.1. The continuous case

This section is devoted to the discrete approximation of the filtering operation associated in the continuous case with a convolution filter. The filtered part $\bar{\phi}$ of a function ϕ is classically defined as

$$\bar{\phi}(x) = \int_{-\infty}^{+\infty} G(x - y)\phi(y)\,\mathrm{d}y, \tag{18}$$

where the convolution kernel G specifies the filter. The operator defined by relation (18) is *a priori* non-local in physical space, and is then worst suited for computations performed with local numerical methods (finite differences, finite elements, finite volumes). So it is necessary to define some local discrete approximations for this operator.

5.2. Approximation by polynomial truncation

A first solution is to build a discrete operator in such a way that the associated continuous differential operator is equivalent up to an arbitrary order to the one of the target filter. To do that, one has to determine the differential operator associated with the convolution filter (18). Introducing the Taylor expansion,

$$\phi(y) = \phi(x) + \sum_{l=1}^{\infty} \frac{(y - x)^l}{l!} \frac{\partial^l \phi(x)}{\partial \xi^l}, \tag{19}$$

and inserting it into relation (18) leads to

$$\bar{\phi}(x) = \phi(x) + \sum_{l=1}^{\infty} \frac{M_l}{l!} \frac{\partial^l \phi(x)}{\partial \xi^l}, \tag{20}$$

where M_l is the moment of order l of the kernel G

$$M_l = \int_{-\infty}^{+\infty} G(\xi) \xi^l \, \mathrm{d}\xi. \tag{21}$$

The differential form (20) is well posed if and only if $|M_l| < \infty \ \forall l$, meaning that the kernel G is rapidly decreasing in space. Let $\bar{\Delta}$ be the characteristic cut-off length-scale associated with the LES filter. Two filters are classically used for theoretical developments in LES, which satisfy that criterion

- the box filter, defined as

$$G(x-y) = \begin{cases} \dfrac{1}{\bar{\Delta}} & \text{if } |x-y| \leq \dfrac{\bar{\Delta}}{2}, \\ 0 & \text{otherwise.} \end{cases} \tag{22}$$

- and the Gaussian filter

$$G(x-y) = \left(\frac{\gamma}{\pi \bar{\Delta}^2}\right)^{1/2} \exp\left(\frac{-\gamma |x-y|^2}{\bar{\Delta}^2}\right). \tag{23}$$

In practice, the real parameter γ is taken equal to 6.

The corresponding differential operators are

- for the box filter

$$\bar{\phi}(x) = \phi(x) + \frac{\bar{\Delta}^2}{24} \frac{\partial^2 \phi(x)}{\partial \xi^2} + \frac{\bar{\Delta}^4}{1920} \frac{\partial^4 \phi(x)}{\partial \xi^4} + \frac{\bar{\Delta}^6}{322\,560} \frac{\partial^6 \phi(x)}{\partial \xi^6} + \frac{\bar{\Delta}^8}{92\,897\,280} \frac{\partial^8 \phi(x)}{\partial \xi^8} + O(\bar{\Delta}^{10}), \tag{24}$$

- for the Gaussian filter

$$\bar{\phi}(x) = \phi(x) + \frac{\bar{\Delta}^2}{24} \frac{\partial^2 \phi(x)}{\partial \xi^2} + \frac{\bar{\Delta}^4}{1152} \frac{\partial^4 \phi(x)}{\partial \xi^4} + \frac{\bar{\Delta}^6}{82\,944} \frac{\partial^6 \phi(x)}{\partial \xi^6} + \frac{\bar{\Delta}^8}{7\,962\,624} \frac{\partial^8 \phi(x)}{\partial \xi^8} + O(\bar{\Delta}^{10}). \tag{25}$$

These differential approximations correspond to linear elliptic filters [19,20]. The associated discrete operator equivalent to the nth order of the convolution filter is obtained by discretizing the differential operators which appear in (24) and (25).

We now illustrate this method on uniform meshes. We introduce the parameter $\epsilon = \bar{\Delta}/\Delta\xi$, which represents the ratio of the mesh size $\Delta\xi$ to the cut-off lengthscale $\Delta\xi$ of the targeted filter.

In order to ensure that the discretized differential operator will effectively be equivalent up to the nth order to the target filter, nth-order-accurate centered discrete operators defined on $(n+1)$-point stencils are used. By discretizing the differential operators, the following discrete operators are derived:

- for the box filter

– operator equivalent to the second-order

$$\bar{\phi}_i = \frac{1}{24}\epsilon^2(\phi_{i+1} + \phi_{i-1}) + \frac{1}{12}(12 - \epsilon^2)\phi_i, \tag{26}$$

– operator equivalent to the fourth-order

$$\bar{\phi}_i = \frac{3\epsilon^4 - 20\epsilon^2}{5760}(\phi_{i+2} + \phi_{i-2}) + \frac{80\epsilon^2 - 3\epsilon^4}{1440}(\phi_{i+1} + \phi_{i-1}) + \frac{3\epsilon^2 - 100\epsilon^2 + 960}{690}\phi_i. \tag{27}$$

- for the Gaussian filter
  – operator equivalent to the second-order

$$\bar{\phi}_i = \frac{1}{24}\epsilon^2(\phi_{i+1} + \phi_{i-1}) + \frac{1}{12}(12 - \epsilon^2)\phi_i, \tag{28}$$

  – operator equivalent to the fourth-order

$$\bar{\phi}_i = \frac{\epsilon^4 - 4\epsilon^2}{1152}(\phi_{i+2} + \phi_{i-2}) + \frac{16\epsilon^2 - \epsilon^4}{288}(\phi_{i+1} + \phi_{i-1}) + \frac{\epsilon^4 - 20\epsilon^2 + 192}{192}\phi_i. \tag{29}$$

5.3. Optimized approximation

A second way to define the discrete operator is to determine its coefficients in such a way that the associated transfer function fits as well as possible with those of the target filter. Whereas the previous method was based on the equivalence up to a given order, the present one relies on an extension of the equivalence for a given wavenumber. Rather than optimizing the choice of the $(2N+1)$ coefficients in order to reduce the error for a finite (and small in practice) set of wavenumbers, it is proposed to minimize the error in a least-square sense over a continuous band of the spectra. The coefficients $\{a_l\}$ will be chosen to minimize the residual I_N, defined as

$$I_N = I(a_{-N}, \ldots, a_0, \ldots, a_N) = \int_0^{\pi/\bar{\Delta}} (\hat{G}(k) - \hat{G}_{\mathrm{d}}(k))^2 \, \mathrm{d}k, \tag{30}$$

where $\hat{G}(k)$ and $\hat{G}_{\mathrm{d}}(k)$ are the transfer functions of the target and the discrete filter respectively. That approach is very close to the ones used to derived discrete differential operators by Tam and Web [21]. As an example, the residual corresponding to the 5-point approximation of the Gaussian filter is

$$I_5 = \int_0^{\pi} \left[\mathrm{e}^{-k^2\bar{\Delta}^2/24} - 2\left(a_2 \cos\left(\frac{2k\bar{\Delta}}{\epsilon}\right) + a_1 \cos\left(\frac{k\bar{\Delta}}{\epsilon}\right) + \frac{a_0}{2}\right)\right]^2 \mathrm{d}(k\bar{\Delta}). \tag{31}$$

It should be noted that the symmetry of the discrete filter (i.e. $a_{-2} = a_2$ and $a_{-1} = a_1$) has been accounted for in that relation. The coefficients computed by this method for the 3- and 5-point approximations of the box filter and the Gaussian filter are given in Table I.

5.4. A priori test on a von Karman spectrum

The various approximations of the convolution filters are tested and qualified considering an ideal von Karman spectrum for the turbulent fluctuations u, which is mathematically defined as

Table I. Optimized coefficients for the Gaussian filter and box filter

	Gaussian filter			Box filter		
	3-point	5-point		3-point	5-point	
	a_1/a_0	a_1/a_0	a_2/a_0	a_1/a_0	a_1/a_0	a_2/a_0
$\epsilon = 1$	0.0763	0.0871	−0.0175	0.079	0.0886	−0.0169
$\epsilon = 2$	0.2527	0.2596	−0.0021	0.274	0.3178	−0.0130
$\epsilon = 3$	1.1160	0.4740	0.0785	1.377	1.0237	0.0368
$\epsilon = 4$	−3.144	0.1036	0.2611	−2.375	2.4414	0.5559
$\epsilon = 5$	−1.102	−0.4252	0.3007	−1.000	0.2949	0.7096
$\epsilon = 6$	−0.809	−0.6134	0.2696	−0.779	−0.5276	0.4437
$\epsilon = 7$	−0.696	−0.6679	0.2419	−0.680	−0.6708	0.3302
$\epsilon = 8$	−0.638	−0.6836	0.2231	−0.627	−0.7003	0.2767
$\epsilon = 9$	−0.604	−0.6873	0.2103	−0.596	−0.7077	0.2532
$\epsilon = 10$	−0.581	−0.6870	0.2014	−0.575	−0.6996	0.2222

$$E(k) = \frac{ak^4}{(b + k^2)^{17/6}}. \tag{32}$$

The selected values for the parameters a and b are 2.682 and 0.417 respectively, so that $\max(E(k)) = E(1) = 1$. Let $\hat{G}(k)$ be the transfer function of the filter. The kinetic energies $\bar{E}(k)$ and $E'(k)$, associated with $\bar{\tilde{u}}'(k)$ and $\hat{u}'(k) = \hat{u} - \bar{\tilde{u}}$ respectively, are given by

$$\bar{E}(k) = \hat{G}^2(k)E(k), \qquad E'(k) = (1 - \hat{G}^2(k))E(k). \tag{33}$$

One can distinguish two spectral domains: the spectral band Ω_1, which contains the modes k such that $0 \le k \le k_c$, where k_c is the cut-off wavenumber associated with the filter, and the spectral band Ω_2, which is composed of the modes k such that $k > k_c$.

The values of the contributions of these two bands to the kinetic energies $\bar{E}$ and E' computed using the 3- and 5-point approximations of the box and Gaussian filters are compared with those obtained using exact continuous filters for two values of the parameter ϵ in Tables II, III, IV and V. The contribution of Ω_1 to $\bar{E}$ was evaluated very accurately in all cases. The level of the measured error concerning the contribution of the spectral band Ω_2 was much greater. Increasing the width of the stencil of the discrete filter and using the optimization procedure to compute its coefficients lead to a significant decrease of that error. The contribution of Ω_1 to E' is satisfactorily evaluated, with the exception of non-optimized 3-point filters, which generate a relative error of the order of 10%. As for $\bar{E}$, the contribution of Ω_2 to E' suffers a large error in all cases except for 5-point filters with $\epsilon = 3$.

Table II. *A priori* tests on von Karman spectra, Gaussian filter, $\epsilon = 2$

	$\bar{E}$		E'	
	Ω_1	Ω_2	Ω_1	Ω_2
Values for continuous filter	3.62018	0.005310	0.001689	0.00751
3-Point filter (error in %)	$+1.33 \times 10^{-3}$	+11.474	−0.963	−14.316
5-Point filter (%)	$+1.33 \times 10^{-3}$	+11.474	−0.963	−14.316
Optimized 3-point filter (%)	-2.92×10^{-3}	+9.912	+0.505	−13.045
Optimized 5-point filter (%)	$+6.64 \times 10^{-4}$	+7.226	+0.118	−10.421

Table III. *A priori* tests on a von Karman spectra, Gaussian filter, $\epsilon = 3$

	$\bar{E}$		E'	
	Ω_1	Ω_2	Ω_1	Ω_2
Values for continuous filter	3.622018	0.00531	0.001689	0.00751
3-Point filter (error in %)	-2.242×10^{-2}	-32.897	$+14.071$	$+59.083$
5-Point filter (%)	$+4.393 \times 10^{-4}$	$+2.933$	-0.316	-3.953
Optimized 3-point filter (%)	$+2.183 \times 10^{-2}$	-19.37	-3.279	$+34.885$
Optimized 5-point filter (%)	$+1.356 \times 10^{-1}$	$+1.21$	-0.061	-1.903

The error is larger for the box filter than for the Gaussian filter. This can be explained by the fact that the transfer function associated with the latter is rapidly decreasing and is more regular than those of the former. It is therefore more easily approximated using fewer degrees of freedom. The transfer functions are shown in Figures 1 and 2.

For the two considered filters, the use of a 5-point filter in conjunction with the optimization procedure for the coefficients gives very good results.

The $\bar{E}(k)$ and $E'(k)$ spectra corresponding to these various cases are shown in Figures 3–9. The analysis of these figures confirms that the error is principally localized in the Ω_2 band.

6. DISCRETE BAND-PASS FILTERS

6.1. Definitions

This section is dedicated to the definition of approximate discrete band-pass filters. Such filters appear when dynamic versions of scale similarity and TKE models are considered, or when 2-filtering level models are coupled to an explicit prefiltering procedure. The desired spectral band corresponds to the interval $[k'_c, k_c]$, with $k'_c = k_c/n$, and the associated velocity field is referred to as $\breve{u}$. The developments will be restricted to the case where only one continuous convolution kernel G is used, without any loss of generality. Two methods are proposed to define a band-pass filter.

The first one is based on the simultaneous use of the filter at the 2-filtering level, the desired spectral band being isolated by a simple subtraction. The resulting field is

$$\breve{u}(k) = \hat{G}_{k'_c}(k)\hat{u}(k) - \hat{G}_{k_c}(k)\hat{u}(k) = (\hat{G}_{k'_c}(k) - \hat{G}_{k_c}(k))\hat{u}(k). \tag{34}$$

The transfer function $\breve{\breve{G}}$ of this band-pass filter is

Table IV. *A priori* tests on a von Karman spectra, box filter, $\epsilon = 2$

	$\bar{E}$		E'	
	Ω_1	Ω_2	Ω_1	Ω_2
Values for continuous filter	3.619609	0.00424	0.001854	0.01023
3-Point filter (error in %)	$+1.718 \times 10^{-2}$	$+47.101$	-9.759	-37.138
5-Point filter (%)	$+2.707 \times 10^{-3}$	$+20.528$	-1.915	-22.443
Optimized 3-point filter (%)	-1.799×10^{-2}	$+30.501$	-1.659	-29.184
Optimized 5-point filter (%)	$+1.449 \times 10^{-3}$	$+11.918$	-0.014	-16.588

Table V. *A priori* tests on a von Karman spectra, box filter, $\epsilon = 3$

	$\bar{E}$		E'	
	Ω_1	Ω_2	Ω_1	Ω_2
Values for continuous filter	3.619609	0.00424	0.001854	0.01023
3-Point filter (error in %)	-6.495×10^{-3}	-11.452	$+3.940$	$+16.711$
5-Point filter (%)	-1.464×10^{-4}	-1.451	$+0.165$	$+2.488$
Optimized 3-point filter (%)	$+6.128\times10^{-3}$	-6.917	-0.535	$+11.685$
Optimized 5-point filter (%)	$+8.48\times10^{-5}$	-0.6733	-0.034	$+1.518$

$$\check{\bar{G}}(k) \equiv \hat{G}_{k'_c}(k) - \hat{G}_{k_c}(k). \tag{35}$$

The energy spectra of $\check{u}(k)$, referred to as $\check{E}(k)$, are

$$\check{E}(k) = \check{\bar{G}}^2(k)E(k) = (\hat{G}_{k'_c}(k) - \hat{G}_{k_c}(k))^2 E(k). \tag{36}$$

The second method consists of the sequential use of the filter at the two levels, giving the following filtered field

$$\check{u}(k) = \hat{G}_{k_c}(k)\hat{u}(k) - \hat{G}_{k'_c}(k)\hat{G}_{k_c}(k)\hat{u}(k) = \hat{G}_{k_c}(k)(1 - \hat{G}_{k'_c}(k))\hat{u}(k). \tag{37}$$

The corresponding transfer function is

$$\check{\bar{G}}(k) = \hat{G}_{k_c}(k)(1 - \hat{G}_{k'_c}(k)), \tag{38}$$

and the resulting energy spectra $\check{E}$ read as

$$\check{E}(k) = \check{\bar{G}}^2(k)E(k) = \hat{G}^2_{k_c}(k)(1 - \hat{G}_{k'_c}(k))^2 E(k). \tag{39}$$

The transfer functions of the band-pass filters computed using both continuous box and Gaussian filters and their various discrete approximations are presented in Figures 10–13. Two cases are considered which correspond to different ratios between the cut-off wavenumber k_0 linked to the mesh size $\Delta\xi$ and the wavenumber k_c. In the first case, the ratio k_0/k_c is set equal

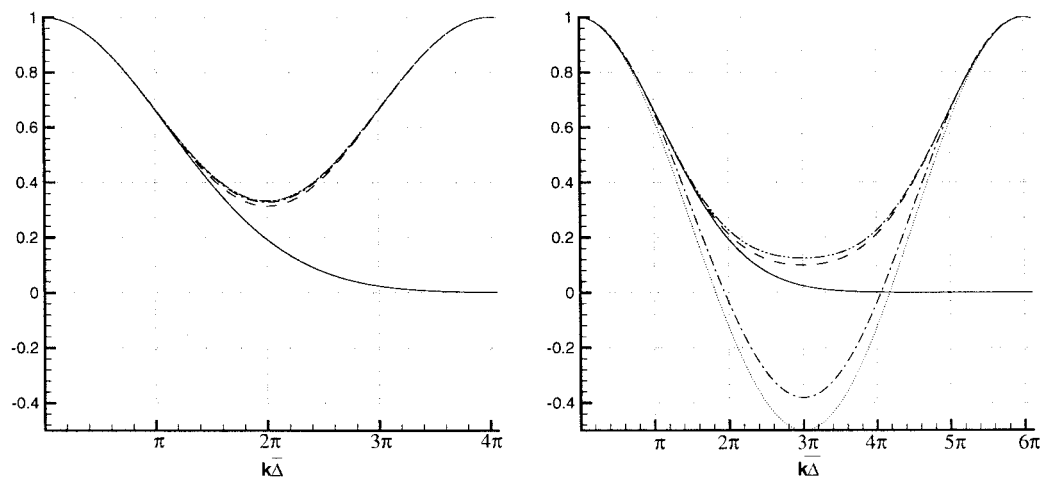

Figure 1. Comparison between transfer functions of 3- and 5-point approximations of the Gaussian filter and the exact solution. Exact, —; 3-point, …; 3-point optimized, -·-·-; 5-point, -···-···-; 5-point optimized - - -.

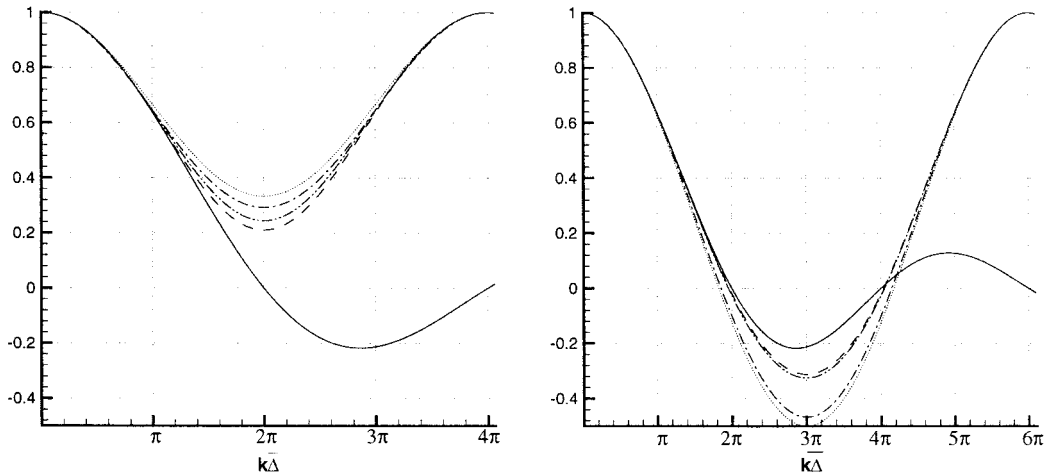

Figure 2. Comparison between transfer functions of 3- and 5-point approximations of the box filter and the exact solution. Exact, —; 3-point, …; 3-point optimized, -·-·-; 5-point, -···-···-; 5-point optimized - - -.

to 2, and so $k_0/k'_c = nk_0/k_c = 4$, and this case will be referred to hereafter as $\epsilon = 2|4$. In the second case, referred to as $\epsilon = 3|6$, we have $k_0/k_c = 3$ and $k_0/k'_c = 6$.

One first notices that, in the continuous case, the Gaussian filter leads to the definition of a strictly positive transfer function, which is monotonotically decreasing for wavenumbers $k > \pi\bar{\Delta}$ for all the considered building procedures. On the other hand, the transfer function resulting from the use of the box filter may take some negative values and does not exhibit a monotonic behavior. Important discrepancies are observed when discrete approximations of this last filter are considered.

In the case $\epsilon = 2|4$, a large overestimation of the contribution of the modes $k > \pi\bar{\Delta}$ is observed with the 3-point filters. This error is significantly reduced when optimized 5-point filters are used. In the case of $\epsilon = 3|6$ an increase of the maximal error on the transfer function is noticed for the large wavenumbers.

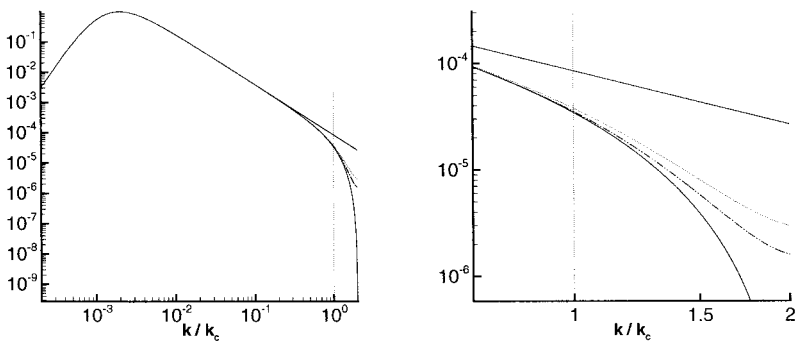

Figure 3. Left: spectra of the filtered part $\bar{E}$ obtained by the application of the box filter and its 3- and 5-point approximations to a von Karman spectrum, in the $\epsilon = 2$ case. Right: enlargement of the $k > k_c$ zone. Exact, —; 3-point, …; 5-point, -···-···-.

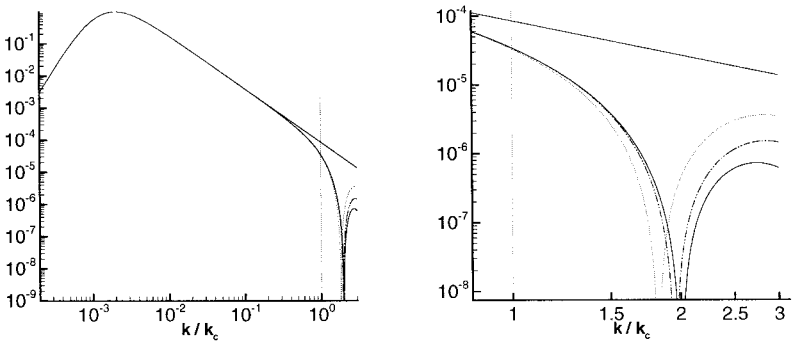

Figure 4. Left: spectra of the filtered part $\bar{E}$ obtained by the application of the box filter and its 3- and 5-point approximations to a von Karman spectrum, in the $\epsilon = 3$ case. Right: enlargement of the $k > k_c$ zone. Exact, —; 3-point, …; 5-point, -···-·-.

6.2. Tests on a von Karman spectrum

The proposed discrete band-pass filters are applied to a von Karman spectrum (32). The two cut-off wavenumbers k'_c and k_c are taken to be equal to 500 and 1000 respectively, i.e. $n = 2$. Two values of the parameter ϵ are used in order to assess the two proposed methods for building band-pass filters. The first one corresponds to the case $\epsilon = 2|4$, and the second one to $\epsilon = 3|6$.

The values of the kinetic energy of the computed velocity fields are compared with those calculated with continuous filters in Table VI for the box filter and in Table VII for the Gaussian filter. Filtered spectra are presented in Figures 14 and 15.

Filters built through simultaneous applications of discrete filters lead to a much larger level of discrepancy than those built through a sequential use of the same filters. In the latter case, the best results are always obtained with the box filter. The use of the optimized 5-point approximate box filter yields a very strong reduction of the error, the strongest being observed for $\epsilon = 3|6$. The building procedure has a strong influence on the error level, as well as on the efficiency of the reduction of this error through the use of optimized coefficients and wider stencils.

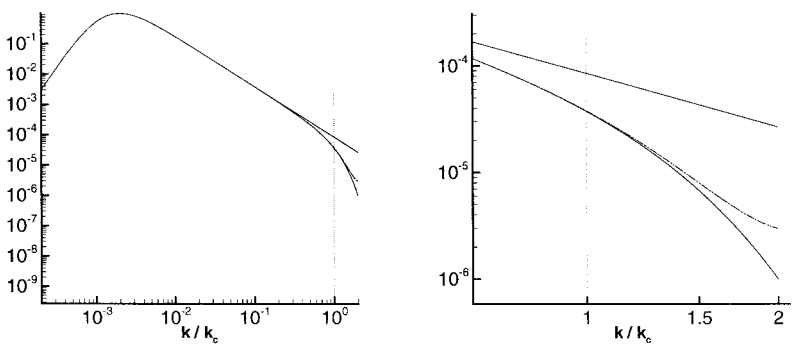

Figure 5. Left: spectra of the filtered part $\bar{E}$ obtained by the application of the Gaussian filter and its 3- and 5-point approximations to a von Karman spectrum, in the $\epsilon = 2$ case. Right: enlargement of the $k > k_c$ zone. Exact, —; 3-point, …; 5-point, -···-·-.

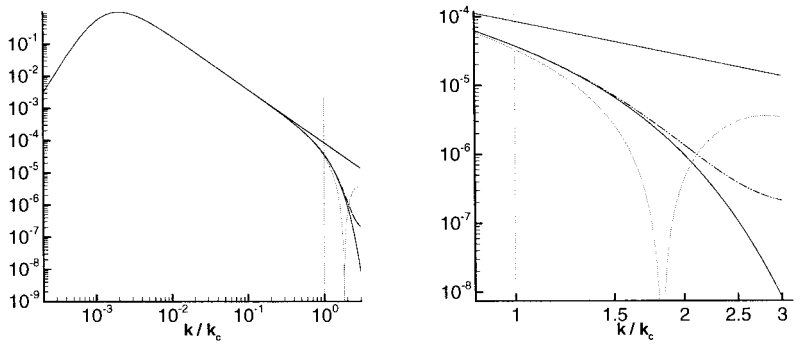

Figure 6. Left: spectra of the filtered part $\bar{E}$ obtained by the application of the Gaussian filter and its 3- and 5-point approximations to a von Karman spectrum, in the $\epsilon = 3$ case. Right: enlargement of the $k > k_c$ zone. Exact, —; 3-point, …; 5-point, -···-·-.

7. SENSITIVITY OF THE SGS MODELS

The dependency of several SGS models which rely on the application of a test filter to its discrete formulation was investigated. The velocity fields obtained by the application LES filter, which is in practice often linked to the computational grid and the numerical error, are referred to as $\bar{u}$. That field represents the information contained in the LES. The field computed by applying a test filter to $\bar{u}$ is referred as $\tilde{\bar{u}}$.

7.1. Selected SGS models

7.1.1. Dynamic Smagorinsky model. The first model studied here is the subgrid viscosity-type model of Smagorinsky, the constant of which is automatically adjusted following the Germano–Lilly [9,10] dynamic procedure. The resulting model reads

$$\tau_{ij} - \frac{1}{3}\tau_{kk}\delta_{ij} = -2\nu_{\mathrm{SGS}}\bar{S}_{ij}, \quad \nu_{\mathrm{SGS}} = C_{\mathrm{D}}\bar{\Delta}^2|\bar{S}|, \tag{40}$$

with

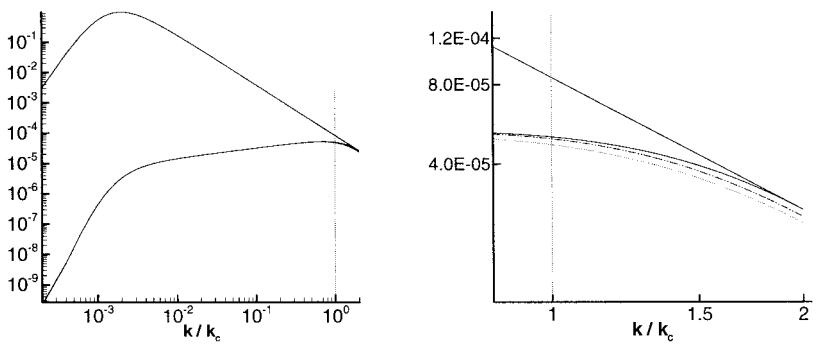

Figure 7. Left: spectra of the fluctuating part E' obtained by the application of the box filter and its 3- and 5-point approximations to a von Karman spectrum, in the $\epsilon = 2$ case. Right: enlargement of the $k > k_c$ zone. Exact, —; 3-point, …; 5-point, -···-·-.

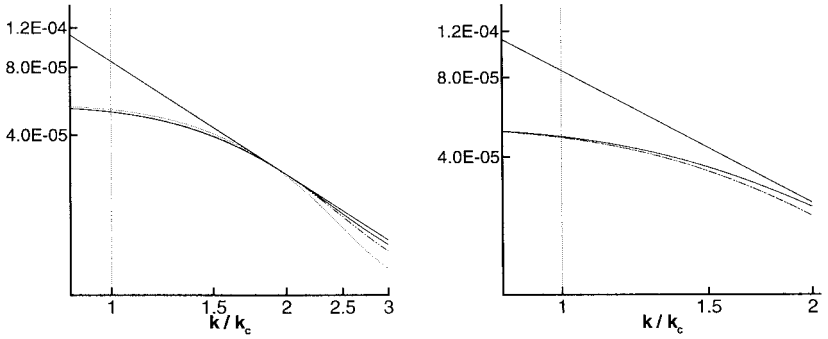

Figure 8. Left: spectra of the fluctuating part E' obtained by the application of the box filter and its 3- and 5-point approximations to a von Karman spectrum, in the $\epsilon = 3$ case (enlargement of the $k > k_c$ zone). Right: idem for the Gaussian filter with $\epsilon = 2$. Exact, —; 3-point, …; 5-point, -···-·-.

$$C_D = \frac{m_{ij}L_{ij}}{m_{lk}m_{lk}}, \tag{41}$$

where tensors m_{ij} and L_{ij} are defined as

$$L_{ij} = \widetilde{\bar{u}_i\bar{u}_j} - \tilde{\bar{u}}_i\tilde{\bar{u}}_j, \tag{42}$$

$$m_{ij} = -2\tilde{\bar{\Delta}}^2|\tilde{\bar{S}}|\tilde{\bar{S}}_{ij} + 2\bar{\Delta}^2\widetilde{|\bar{S}|\bar{S}_{ij}}. \tag{43}$$

7.1.2. MSM and modified MSM. The MSM, proposed by Sagaut [4], accounts for the contribution of the resolved field gradients, of the kinetic energy of the highest resolved modes and the cut-off length-scale $\bar{\Delta}$.

The subgrid viscosity is defined as

$$\nu_{SGS} = C_M|\bar{S}|^{1/2}(q_c^2)^{1/4}\bar{\Delta}^{3/2}, \tag{44}$$

where $q_c^2 = \frac{1}{2}\bar{u}_i'\bar{u}_i'$ is the kinetic energy of the test field $\bar{u}' = \bar{u} - \tilde{\bar{u}}$. The value of the constant C_M computed using the EDQNM closure is 0.08.

Considering the ideal case, where the grid and test filters respectively associated with the wavenumbers k_c and k_c' are sharp Fourier filters and where the inertial range of the spectra is infinite, the quantity q_c^2 may be easily linked to the SGS kinetic energy E_{SGS}

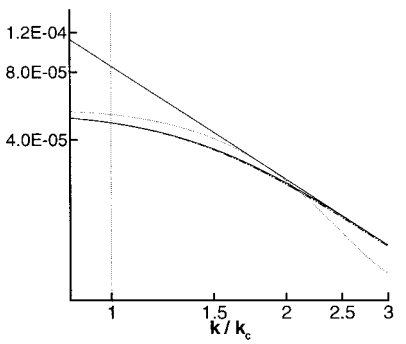

Figure 9. Spectra of the fluctuating part E' obtained by the application of the Gaussian filter and its 3- and 5-point approximations to a von Karman spectrum, in the $\epsilon = 3$ case (enlargement of the $k > k_c$ zone). Exact, —; 3-point, …; 5-point, -···-·-.

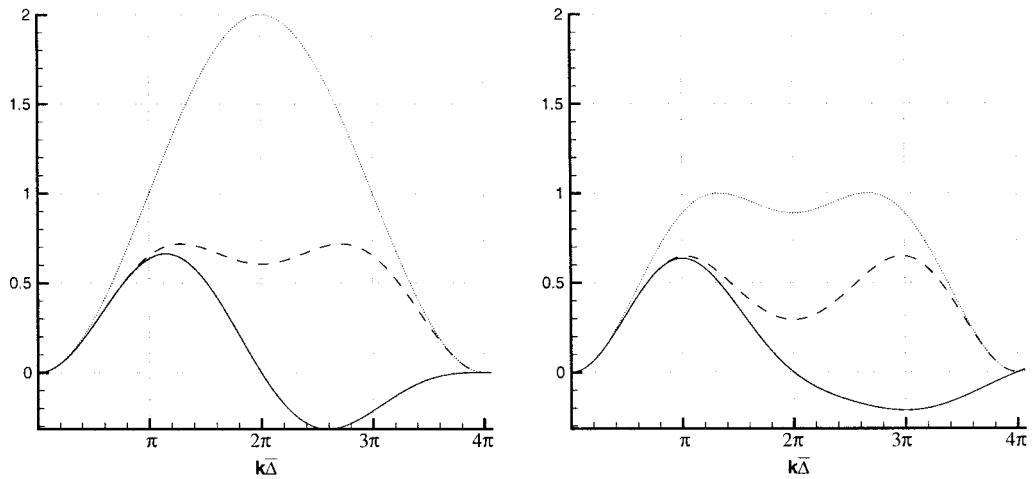

Figure 10. Transfer functions of band-pass filters defined using the box filter and its discrete approximations for $\epsilon = 2|4$. Left: simultaneous filtering; right: sequential filtering. Exact, —; 3-point, …; 5-point, -···-·-.

$$q_c^2 \int_{k_c'}^{k_c} K_0 \epsilon^{2/3} k^{-5/3}\, \mathrm{d}k, \qquad E_{\mathrm{SGS}} = \int_{k_c}^{\infty} K_0 \epsilon^{2/3} k^{-5/3}\, \mathrm{d}k, \tag{45}$$

where K_0 and ϵ are respectively the Kolmogorov constant and the kinetic energy dissipation rate. Simple calculations lead to

$$q_c^2 = \beta(k_c', k_c) E_{\mathrm{SGS}}, \qquad \beta(k_c', k_c) = \left[\left(\frac{k_c'}{k_c} \right)^{-2/3} - 1 \right]. \tag{46}$$

To account for this relationship, the basic MSM (44) is modified as

$$\nu_{\mathrm{SGS}} = C_M |\bar{S}|^{1/2} (q_c^2)^{1/4} \bar{\Delta}^{3/2} \beta(k_c', k_c)^{-1/4}. \tag{47}$$

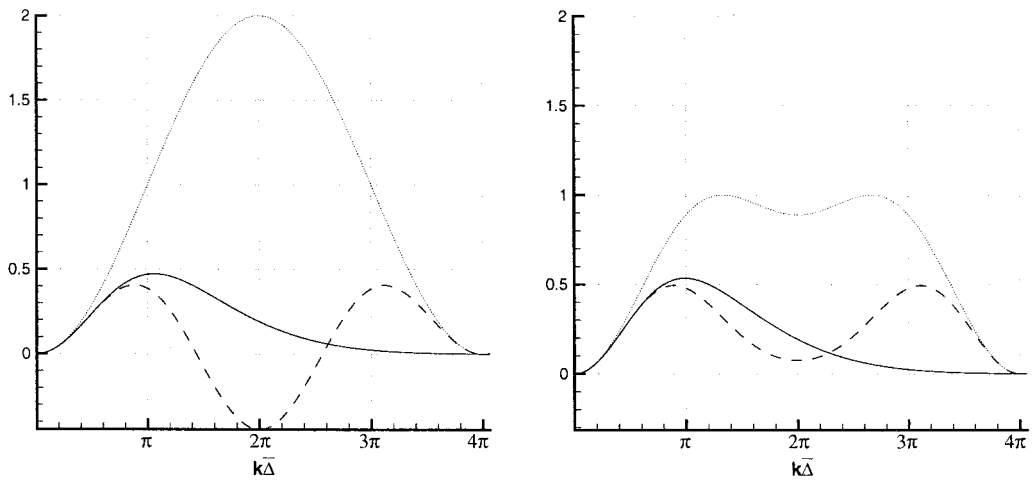

Figure 11. Transfer functions of band-pass filters defined using the Gaussian filter and its discrete approximations for $\epsilon = 2|4$. Left: simultaneous filtering; right: sequential filtering. Exact, —; 3-point, …; 5-point, -···-·-.

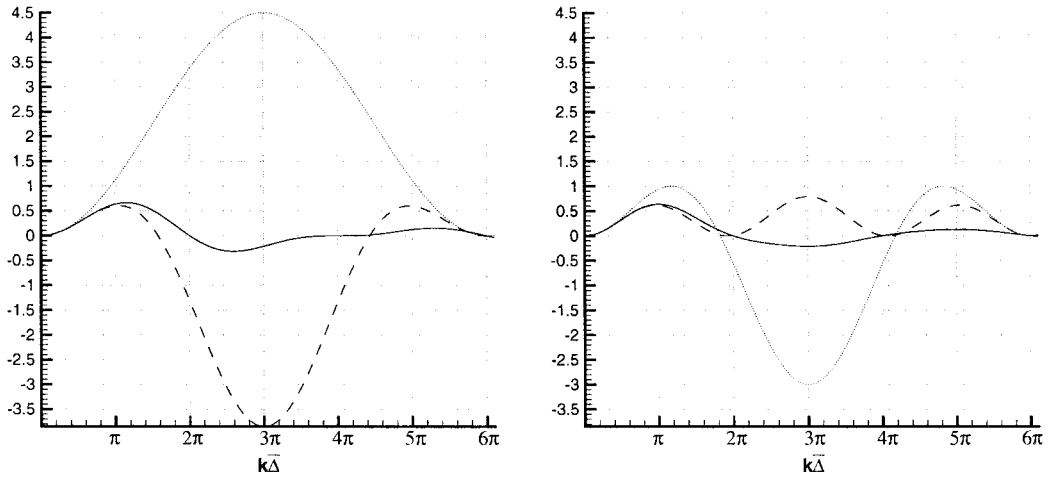

Figure 12. Transfer functions of band-pass filters defined using the box filter and its discrete approximations for $\epsilon = 3|6$. Left: simultaneous filtering; right: sequential filtering. Exact, —; 3-point, …; 5-point, -···-·-.

This new improved formulation allows one to account explicitly for the cut-off wavenumber of the test filter, resulting in a better adaptation of the model to the local state of the resolved field. One can notice that both quantities q_c^2 and E_{SGS} are equal if $k'_c = k_c/\sqrt{8}$.

7.1.3. Selective MSM. In order to provide a better capturing of the large-scale intermittency, David (see [7,22]) proposed a structural sensor based on the evaluation of the local angular fluctuation θ of the rotational of the test field $\bar{\omega}'$, which allows the SGS model to vanish when the three-dimensional features of the highest resolved frequencies do not correspond to the phenomenology of developed isotropic homogeneous turbulence.

If the angle θ is smaller than a threshold angle θ_0, one will assume that all the dynamically active scales are captured by the simulation and the SGS model will be set to zero. The selective MSM is obtained by multiplying the MSM by the selection function $f_{\theta_0}(\theta)$

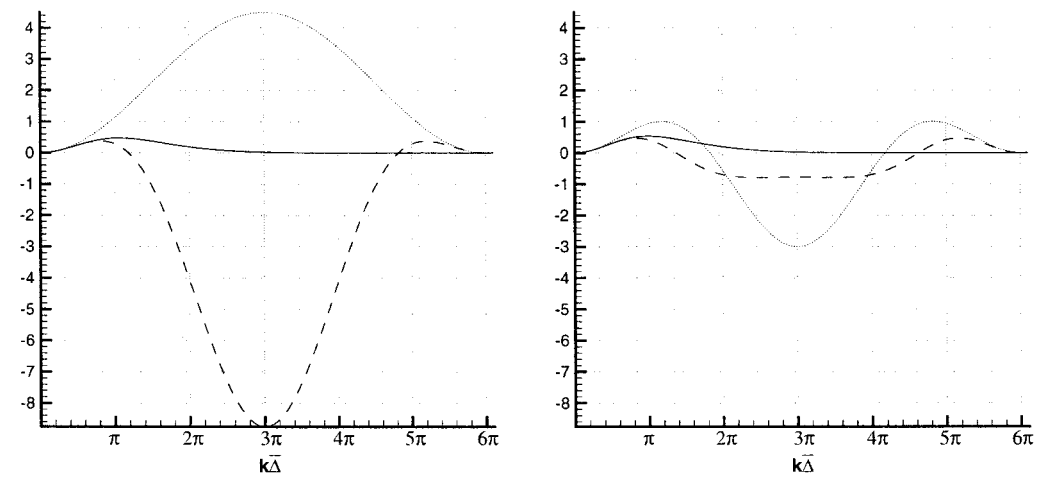

Figure 13. Transfer functions of band-pass filters defined using the Gaussian filter and its discrete approximations for $\epsilon = 3|6$. Left: simultaneous filtering; right: sequential filtering. Exact, —; 3-point, …; 5-point, -···-·-.

Table VI. Errors between the kinetic energy of the field computed using the discrete band-pass box filter and the corresponding continuous filter

	$\epsilon = 2\|4$		$\epsilon = 3\|6$	
	Simultaneous	Sequential	Simultaneous	Sequential
Exact value	0.010145	0.010832	0.01049	0.01095
Error in %:				
3-Point filter	+353.03	+123.14	+1591.78	+330.5
Optimized 3-point filter	+277.49	+83.51	+1317.6	+249.25
5-Point filter	+34.01	+13.70	+546.35	+4.38
Optimized 5-point filter	+25.77	+8.68	+466.39	+2.79

$$v_{\mathrm{SGS}} = C'_M |\bar{S}|^{1/2} (q_c^2)^{1/4} \bar{\Delta}^{3/2} f_{\theta_0}(\theta), \tag{48}$$

with

$$f_{\theta_0}(\theta) = \begin{cases} 1 & \text{if } \theta > \theta_0 \\ 0 & \text{otherwise} \end{cases}. \tag{49}$$

Following David, the constant is evaluated as $C'_M = 1.65 \times C_M$, and the threshold angle θ_0 is taken to be equal to 20°.

7.1.4. Liu–Meneveau–Katz similarity model and modified Liu–Meneveau–Katz model. The similarity SGS models are based on the hypothesis that the statistical structure of a turbulent field is slowly and continuously varying in frequency, and approximate the subgrid stress tensor τ_{ij} via an extrapolation in frequency. That hypothesis, which has been assessed by experiments, is justified by the non-locality of vortical structures on a Fourier basis [13]. Following the original idea of Bardina *et al.* [3], Liu *et al.* [13] propose the new Liu–Meneveau–Katz (LMK) similarity model

$$\tau_{ij} = C_{\mathrm{L}} (\widetilde{\bar{u}_i \bar{u}_j} - \tilde{\bar{u}}_i \tilde{\bar{u}}_j) = C_{\mathrm{L}} L_{ij}, \tag{50}$$

where $C_{\mathrm{L}} = 0.45 \pm 0.15$. Like the basic version of the MSM, this model does not depend explicitly on the cut-off frequencies associated with the grid and test filter. We propose here an improvement of the LMK model, derived in the same spirit as for the MSM, in order to ensure that the trace of the parametrized SGS tensor will be equal to the SGS kinetic energy, using the same hypotheses as previously. We have

Table VII. Errors between the kinetic energy of the field computed using the discrete band-pass Gaussian filter and the corresponding continuous filter

	$\epsilon = 2\|4$		$\epsilon = 3\|6$	
	Simultaneous	Sequential	Simultaneous	Sequential
Exact value	0.006412	0.00883	0.00618	0.00890
Error in %:				
3-Point filter	+616.83	+173.54	+2639.25	+429.67
Optimized 3-point filter	+421.89	+115.152	+1902.5	+224.28
5-Point filter	−18.64	−25.56	+7863.8	+87.35
Optimized 5-point filter	−23.47	−17.61	+4918.2	+23.62

Table VIII. Averaged values of the dynamic constant, the SGS viscosity and the SGS dissipation computed with the dynamic model

	$\epsilon = 2$			$\epsilon = 3$		
	$\langle \nu_{SGS} \rangle$	c_d	$\langle \lvert D_{SGS} \rvert \rangle$	$\langle \nu_{SGS} \rangle$	c_d	$\langle \lvert D_{SGS} \rvert \rangle$
3-Point filter	2.322×10^{-4}	1.188×10^{-2}	2.382×10^{-2}	2.065×10^{-4}	1.056×10^{-2}	2.118×10^{-2}
Gaussian 5-point filter	1.530×10^{-4}	7.829×10^{-3}	1.570×10^{-2}	1.083×10^{-4}	5.541×10^{-3}	1.111×10^{-2}
Box 5-point filter	1.545×10^{-4}	7.902×10^{-3}	1.584×10^{-2}	1.099×10^{-4}	5.624×10^{-3}	1.128×10^{-2}
Gaussian optimized 3-point filter	2.341×10^{-4}	1.197×10^{-2}	2.401×10^{-2}	1.915×10^{-4}	9.699×10^{-3}	1.965×10^{-2}
Box optimized 3-point filter	2.467×10^{-4}	1.262×10^{-2}	2.531×10^{-2}	2.025×10^{-4}	1.036×10^{-2}	2.077×10^{-2}
Gaussian optimized 5-point filter	1.529×10^{-4}	7.821×10^{-3}	1.568×10^{-2}	1.083×10^{-4}	5.539×10^{-3}	1.1108×10^{-2}
Box optimized 5-point filter	1.512×10^{-4}	7.886×10^{-3}	1.581×10^{-2}	1.127×10^{-4}	5.623×10^{-3}	1.127×10^{-2}

$$L_{kk} = \bar{u}'_i \bar{u}'_i = 2q_c^2 = 2 \int_{k'_c}^{k_c} K_0 \epsilon^{2/3} k^{-5/3} \, \mathrm{d}k = 2\beta(k'_c, k_c) E_{SGS}. \tag{51}$$

An improved version of the model (50) is

$$\tau_{ij} = C_L L_{ij}, \quad C_L = \frac{1}{2\beta(k'_c, k_c)}. \tag{52}$$

One may remark that in the case of $\beta(k'_c, k_c) = 1$ the computed value of the constant C_L is very close to the empirical initial value.

7.2. A priori tests

The dependency of the SGS models to the test filter is now investigated through some *a priori* tests which were carried out using the same velocity field u issued from an LES of isotropic homogeneous turbulence on a 128^3 grid [E. Garnier, private communication]. The cut-off length scale of the LES filter is classically associated with the mesh size of the computational grid $\bar{\Delta} = \Delta\xi$, and the cut-off length scale of the test filter is then specified by choosing the value of the parameter ϵ. It should be noted that the exact nature of the LES filter remains unknown.

Fourteen different cases are considered for each SGS model, which correspond to various 3- and 5-point approximations of both Gaussian and box filters, for $\epsilon = 2$ and $\epsilon = 3$.

The mean values, computed from the 128^3 samples, of the dynamic constant, the associated SGS viscosity ν_{SGS} and SGS dissipation D_{SGS}, defined as

$$D_{SGS} = -\tau_{ij} \bar{S}_{ij}, \tag{53}$$

are presented in Table VIII. One observes that the use of 5-point filters leads to a large reduction of the computed value of the dynamic constant, inducing a similar decrease of the

mean SGS dissipation $\langle D_{\mathrm{SGS}} \rangle$. The values of the three parameters exhibit a larger dispersion with $\epsilon = 3$ than with $\epsilon = 2$, the smallest dissipation being found in the former case. For all the cases, the use of the optimization procedure to compute the coefficients of the discrete filter produces only a weak decrease of the dissipation.

The averaged values of the kinetic energy of the test field, the SGS viscosity, and the SGS dissipation computed using the MSM are given in Table IX. The SGS viscosity and dissipation for the MSM model are approximately ten times larger than for the dynamic model. One remarks that the relative dispersion is lower than for the dynamic model. However, as in the previous case, the dissipation computed with 5-point filters is smaller than with 3-point filters. On the other hand, the dissipation is higher for $\epsilon = 3$ than for $\epsilon = 2$. This can be explained by the fact that the test field contains more kinetic energy because its spectral support is wider, inducing an increase of the SGS viscosity.

Results obtained with the modified MSM are presented in Table X. The modification has the desired effect: the discrepancies between the two cases $\epsilon = 2$ and $\epsilon = 3$ are smaller than for the original model. The trends are the same as for the previous cases: the use of discrete test filters which are more local in spectral space yields a decrease of the energy transfer from resolved scales towards subgrid scales. It should be noted that the improvement is limited, because the correction factor appears as $\beta^{-1/4}$ and not as β^{-1}: the effective power of the factor concentrates the values around 1. More precisely, the correction factor is equal to 1.142 and 0.980 for $\epsilon = 2$ and $\epsilon = 3$ respectively.

The results obtained with the selective MSM are shown in Table XI. The selection function, by reducing the support of the SGS viscosity, leads to a significant decrease of the associated dissipation. This selection function is very sensitive to the choice for ϵ and the filter, or equivalently to the structure of the test field. On the one hand, a larger value of ϵ corresponds to a higher dissipation level than for the basic MSM, but on the other hand, the use of a 5-point filter and optimized coefficients may also lead to an increase of the SGS dissipation. In the case $\epsilon = 2$, the SGS dissipation level is close to the one computed with the dynamic model.

Table IX. Averaged values of the test field's kinetic energy, the SGS viscosity and of SGS dissipation computed with the MSM

	$\epsilon = 2$			$\epsilon = 3$		
	$\langle q_c^2 \rangle$	$\langle \nu_{\mathrm{SGS}} \rangle$	$\langle \lvert D_{\mathrm{SGS}} \rvert \rangle$	$\langle q_c^2 \rangle$	$\langle \nu_{\mathrm{SGS}} \rangle$	$\langle \lvert D_{\mathrm{SGS}} \rvert \rangle$
3-Point filter	3.086×10^{-3}	1.439×10^{-3}	1.369×10^{-1}	1.254×10^{-2}	2.048×10^{-3}	1.931×10^{-1}
Gaussian 5-point filter	3.723×10^{-3}	1.432×10^{-3}	1.354×10^{-1}	1.077×10^{-2}	1.894×10^{-3}	1.775×10^{-1}
Box 5-point filter	3.912×10^{-3}	1.448×10^{-3}	1.371×10^{-1}	1.151×10^{-2}	1.924×10^{-3}	1.803×10^{-1}
Gaussian optimized 3-point filter	3.127×10^{-3}	1.444×10^{-3}	1.374×10^{-1}	1.095×10^{-2}	1.980×10^{-3}	1.868×10^{-1}
Box optimized 3-point filter	3.137×10^{-3}	1.479×10^{-3}	1.406×10^{-1}	1.210×10^{-2}	2.030×10^{-3}	1.914×10^{-1}
Gaussian optimized 5-point filter	3.741×10^{-3}	1.433×10^{-3}	1.356×10^{-1}	1.079×10^{-2}	1.895×10^{-3}	1.775×10^{-1}
Box optimized 5-point filter	3.912×10^{-3}	1.450×10^{-3}	1.373×10^{-1}	1.150×10^{-2}	1.923×10^{-3}	1.803×10^{-1}

Table X. Averaged values of the test field's kinetic energy, the SGS viscosity and the SGS dissipation computed with the modified MSM

	$\epsilon = 2$			$\epsilon = 3$		
	$\langle q_c^2 \rangle$	$\langle v_{SGS} \rangle$	$\langle \lvert D_{SGS} \rvert \rangle$	$\langle q_c^2 \rangle$	$\langle v_{SGS} \rangle$	$\langle \lvert D_{SGS} \rvert \rangle$
3-Point filter	3.086×10^{-3}	1.643×10^{-3}	1.563×10^{-1}	1.254×10^{-2}	2.009×10^{-3}	1.894×10^{-1}
Gaussian 5-point filter	3.723×10^{-3}	1.635×10^{-3}	1546×10^{-1}	1.077×10^{-2}	1.858×10^{-3}	1.741×10^{-1}
Box 5-point filter	3.912×10^{-3}	1.654×10^{-3}	1.566×10^{-1}	1.151×10^{-2}	1.887×10^{-3}	1.768×10^{-1}
Gaussian optimized 3-point filter	3.127×10^{-3}	1.650×10^{-3}	1569×10^{-1}	1.095×10^{-2}	1.912×10^{-3}	1.832×10^{-1}
Box optimized 3-point filter	3.437×10^{-3}	1.689×10^{-3}	1.606×10^{-1}	1.210×10^{-2}	1.991×10^{-3}	1.877×10^{-1}
Gaussian optimized 5-point filter	3.741×10^{-3}	1.636×10^{-3}	1.519×10^{-1}	1.079×10^{-2}	1.858×10^{-3}	1.711×10^{-1}
Box optimized 5-point filter	3.942×10^{-3}	1.656×10^{-3}	1.568×10^{-1}	1.150×10^{-2}	1.886×10^{-3}	1.768×10^{-1}

Mean values of the SGS dissipation computed using the basic and modified LMK similarity models are given in Table XII. When using the basic model, one notices first that a widening of the spectral band associated with the test filter induces a large increase of the SGS dissipation, as observed with the MSM. The dispersion of the values is larger for $\epsilon = 3$ than for $\epsilon = 2$, indicating that the model is very sensitive to the transfer function of the discrete test filter. The use of the 5-point filter and the optimization procedure lead to a decrease of the SGS dissipation, as in the previous cases. The level of dissipation found with $\epsilon = 2$ is similar

Table XI. Averaged values of the test field's kinetic energy, the SGS viscosity and the SGS dissipation computed with the selective MSM

	$\epsilon = 2$			$\epsilon = 3$		
	$\langle q_c^2 \rangle$	$\langle v_{SGS} \rangle$	$\langle \lvert D_{SGS} \rvert \rangle$	$\langle q_c^2 \rangle$	$\langle v_{SGS} \rangle$	$\langle \lvert D_{SGS} \rvert \rangle$
3-Point filter	3.086×10^{-3}	8.323×10^{-5}	7.163×10^{-3}	1.254×10^{-2}	6.966×10^{-4}	6.381×10^{-2}
Gaussian 5-point filter	3.723×10^{-3}	1.503×10^{-4}	1.123×10^{-2}	1.077×10^{-2}	5.643×10^{-4}	5.434×10^{-2}
Box 5-point filter	3.912×10^{-3}	1.661×10^{-4}	1.577×10^{-2}	1.151×10^{-2}	6.296×10^{-4}	6.073×10^{-2}
Gaussian optimized 3-point filter	3.127×10^{-3}	8.517×10^{-5}	7.331×10^{-3}	1.095×10^{-2}	5.813×10^{-4}	5.298×10^{-2}
Box optimized 3-point filter	3.137×10^{-3}	9.952×10^{-5}	8.596×10^{-3}	1.210×10^{-2}	6.643×10^{-4}	6.075×10^{-2}
Gaussian optimized 5-point filter	3.711×10^{-3}	1.526×10^{-4}	1.445×10^{-2}	1.079×10^{-2}	5.670×10^{-4}	5.460×10^{-2}
Box optimized 5-point filter	3.942×10^{-3}	1.698×10^{-4}	1.614×10^{-2}	1.150×10^{-2}	6.282×10^{-4}	6.060×10^{-2}

Table XII. Averaged value of the SGS dissipation $\langle |D_{SGS}| \rangle$ computed with the LMK and modified LMK similarity models

	LMK		Modified LMK	
	$\epsilon = 2$	$\epsilon = 3$	$\epsilon = 2$	$\epsilon = 3$
3-Point filter	2.807×10^{-2}	5.345×10^{-2}	2.389×10^{-2}	2.474×10^{-2}
Gaussian 5-point filter	2.425×10^{-2}	3.764×10^{-2}	2.064×10^{-2}	1.742×10^{-2}
Box 5-point filter	2.490×10^{-2}	3.905×10^{-2}	2.119×10^{-2}	1.807×10^{-2}
Gaussian optimized 3-point filter	2.825×10^{-2}	5.050×10^{-2}	2.101×10^{-2}	2.338×10^{-2}
Box optimized 3-point filter	2.955×10^{-2}	5.272×10^{-2}	2.549×10^{-2}	2.440×10^{-2}
Gaussian optimized 5-point filter	2.433×10^{-2}	3.770×10^{-2}	2.070×10^{-2}	1.745×10^{-2}
Box optimized 5-point filter	2.503×10^{-2}	3.902×10^{-2}	2.130×10^{-2}	1.806×10^{-2}

to the one computed with the dynamic model. An important effect of the proposed modification is observed: the level of discrepancy between the $\epsilon = 2$ and $\epsilon = 3$ cases is reduced, and the SGS dissipation is smaller in the latter case. Here, a wider test spectral band is associated with a smaller amplitude of the SGS terms, as for the dynamic model. The level of dissipation level is very close to the one computed with the dynamic model for the two selected values of ϵ. The reduction is larger when 5-point filters are used. The improvement is more significant than the one noticed for the MSM, because the correction factor now appears as β^{-1}.

The observed decrease of the SGS dissipation when using a 5-point filter and optimized coefficients results from the reduction of the error incurred by the transfer function concerning the contribution of the low frequencies to the test field. A better spectral localization of the test field renders the SGS models more sensitive to the local state of the flow and allows for accounting of the large-scale intermittency in a better way. It induces a reduction of the support of the SGS models and the associated dissipation, or in an equivalent manner to an increase of the SGS dissipation intermittency. The proposed modifications of the MSM and LMK models, based on the normalization of the trace of the SGS tensor, lead to the definition of improved models which are less sensitive to the spectral width of the test filter. The present tests show that the dynamic procedure partially reduces the dependency on the test filter. Figures 16–19 show the iso-values of the SGS dissipation D_{SGS} computed with the dynamic model using discrete approximations of the Gaussian filter. The increase of the SGS

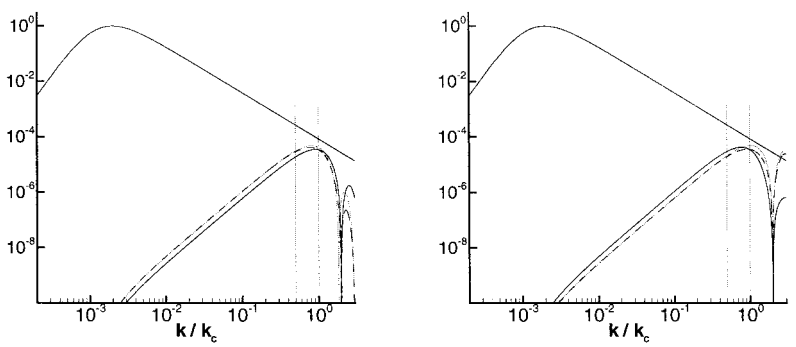

Figure 14. Energy spectrum of the field obtained by applying a band-pass filter based on the box filter to a von Karman spectrum in the $\epsilon = 3$ case. Left: simultaneous filtering; right: sequential filtering. Exact, —; 3-point, …; 5-point, -···-·-.

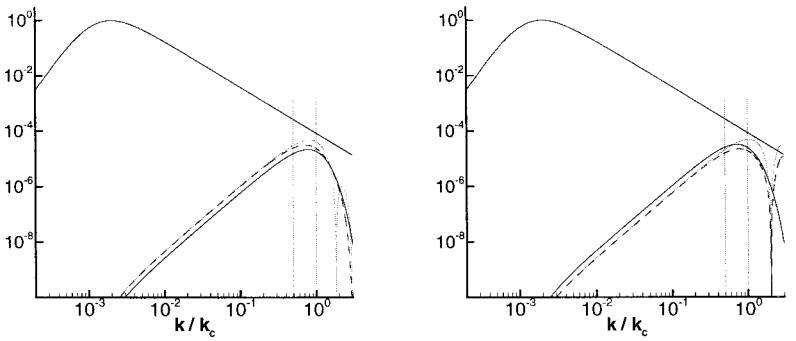

Figure 15. Energy spectrum of the field obtained by applying a band-pass filter based on the Gaussian filter to a von Karman spectrum, in the $\epsilon = 3$ case. Left: simultaneous filtering; right: sequential filtering. Exact, —; 3-point, …; 5-point, -···-···-.

intermittency due to better spectral properties of the discrete test filter is observed when comparing these figures. One can notice that 3-point filters lead to similar results for the two values of ϵ, whereas a 5-point filter produces a clear reduction of the support of the dissipation.

8. CONCLUSIONS

The general form of the discrete filter in the uniform one-dimensional case has been derived and analyzed, as well as the associated transfer function and continuous equivalent differential operator. Equivalence classes for the discrete filters have been proposed: the first one relies on the equality of the transfer function for a given wavenumber, and the second one on the

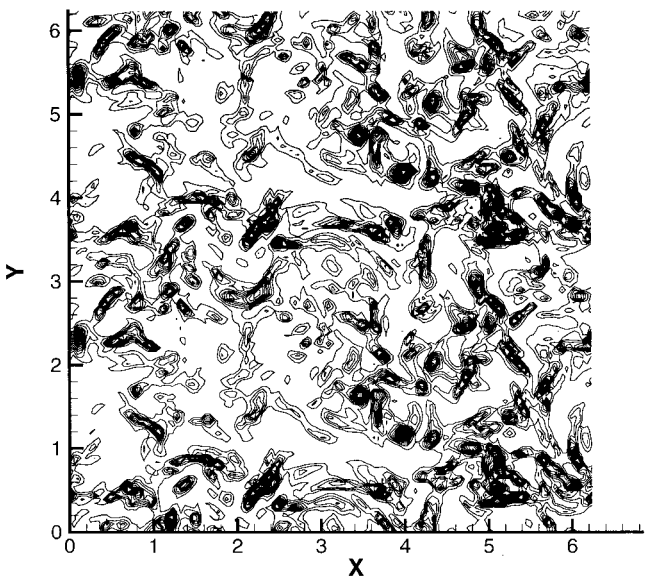

Figure 16. Iso-value contours of the SGS dissipation in a plane, computed with the dynamic model, using a discrete 3-point Gaussian test filter, standard coefficients, with $\epsilon = 2$.

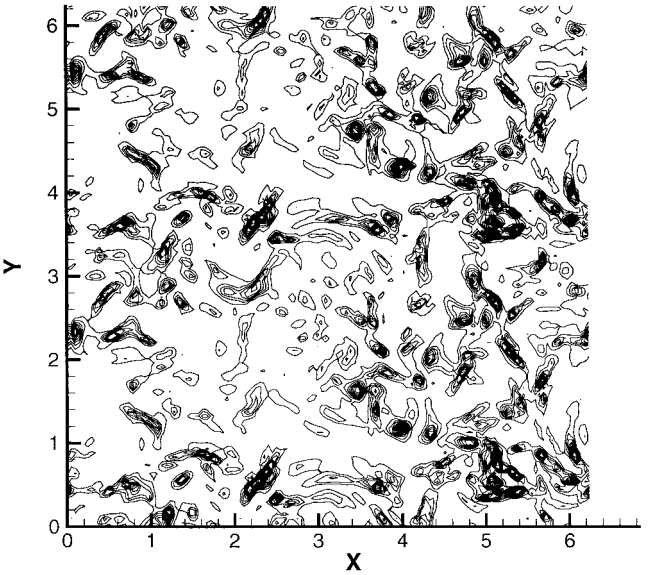

Figure 17. Iso-value contours of the SGS dissipation in a plane, computed with the dynamic model, using a discrete 5-point Gaussian test filter, optimized coefficients, with $\epsilon = 2$.

equivalence up to a given order of the associated differential operators. Several methods to extend discrete filters to the multi-dimensional case, based on the equivalence class concept, are proposed. The generalization to curvilinear structured and unstructured meshes is also discussed.

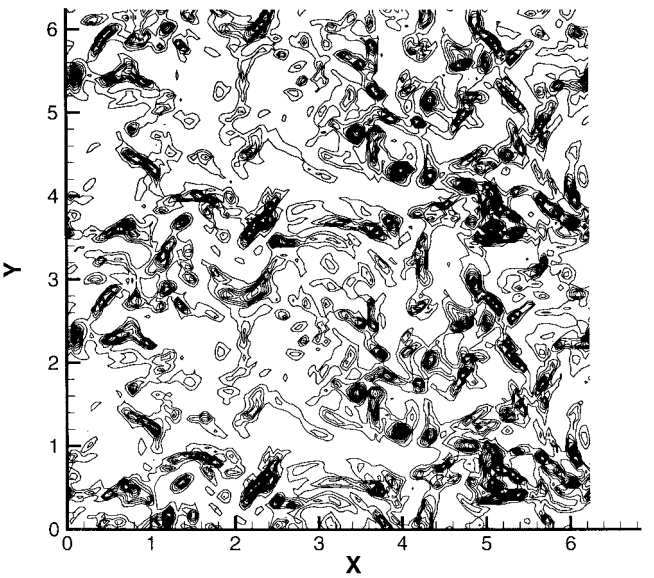

Figure 18. Iso-value contours of the SGS dissipation in a plane, computed with the dynamic model, using a discrete 3-point Gaussian test filter, standard coefficients, with $\epsilon = 3$.

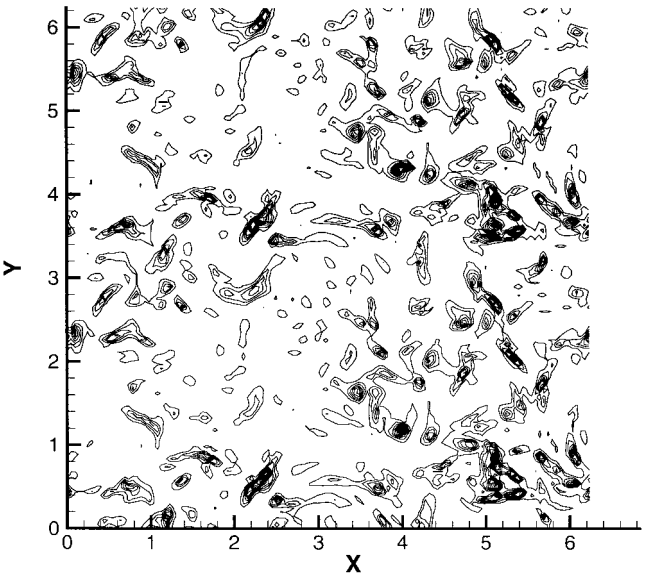

Figure 19. Iso-value contours of the SGS dissipation in a plane. computed with the dynamic model, using a discrete 5-point Gaussian test filter, optimized coefficients, with $\epsilon = 3$.

Discrete approximations of convolution filters, which best fit to the continuous filter in a given sense, are detailed. Discrete operators corresponding to the Gaussian and box filters are given and tested on a von Karman spectrum. The tests demonstrate the efficiency of the proposed optimization procedure to compute the coefficients of the discrete filter. The use of 5-point filters leads to a clear improvement in results over the 3-point filters.

The defined discrete filters are then used as a basic tool to build up some band-pass filters. Two methods are proposed: the first one consists of a sequential application of the filters, and the second one consists of a simultaneous use of the discrete filters. *A priori* tests on a von Karman spectrum show that the former produces the most accurate results, the best accuracy being obtained using discrete approximations of the box filter.

Finally, the dependency of SGS models has been tested through *a priori* testing on a velocity field issued from the large-eddy simulation of isotropic homogeneous turbulence on a 128^3 grid. Several models are considered: the dynamic model, the MSM and its selective variant, and the LMK similarity model. Improved versions of the MSM and the LMK model are proposed, which account for the spectral width of the test filter. All the models exhibit a sensitivity on the discrete test filter. This sensitivity is less pronounced for models which have a self-adjustment capability, like the dynamic model and the proposed improved LMK and MSM models. The smallest dissipation levels are achieved when using discrete filters which have the most local transfer functions, in accordance with the previous results of Najjar and Tafti [17]. These filters minimize the error induced on the low frequencies contribution to the test field. The most efficient filters are 5-point filters whose coefficients are computed using the proposed optimization procedure.

ACKNOWLEDGMENTS

This work was supported by ONERA/PRF M2NT under Grant 1145A337A.

REFERENCES

1. R.S. Rogallo and P. Moin, 'Numerical simulation of turbulent flows', *Annu. Rev. Fluid Mech.*, **16**, 99–137 (1984).
2. P. Sagaut, *Introduction à la Simulation des Grandes Échelles des Écoulements de Fluide Incompressible*, Springer, Berlin, 1998.
3. J. Bardina, J.H. Ferziger and W.C. Reynolds, 'Improved turbulence models based on large-eddy simulation of homogeneous, incompressible, turbulent flows', *Report TF-19*, Thermosciences Division, Department of Mechanical Engineering, Stanford University, 1983.
4. P. Sagaut, 'Numerical simulations of separated flows with subgrid models', *Rech. Aéro.*, 1–63 (1996).
5. A.J. Smagorinsky, 'General circulation experiments with the primitive equations', *Mon. Weather Rev.*, **91**, 99–164 (1963).
6. O. Métais and M. Lesieur, 'Spectral large-eddy simulation of isotropic and stably stratified turbulence', *J. Fluid Mech.*, **239**, 157–194 (1992).
7. M. Lesieur and O. Métais, 'New trends in large-eddy simulations of turbulence', *Annu. Rev. Fluid Mech.*, **28**, 45–82 (1996).
8. F. Ducros, P. Comte and M. Lesieur, 'Large-eddy simulation of transition to turbulence in a boundary layer developing spatially over a flat plate', *J. Fluid Mech.*, **326**, 1–36 (1996).
9. M. Germano, U. Piomelli, P. Moin and W.H. Cabot, 'A dynamic subgrid-scale eddy viscosity model', *Phys. Fluids A*, **3**, 1760–1765 (1991).
10. D.K. Lilly 'A proposed modification of the Germano subgrid-scale closure method', *Phys. Fluids A*, **4**, 633–635 (1992).
11. C. Meneveau, T.S. Lund and W.H. Cabot, 'A Lagrangian dynamic subgrid-scale model of turbulence', *J. Fluid Mech.*, **319**, 353–385 (1991).
12. S. Ghosal, T.S. Lund, P. Moin and K. Akselvoll, 'A dynamic localization model for large-eddy simulation of turbulent flows', *J. Fluid Mech.*, **286**, 229–255 (1995).
13. S. Liu. C. Meneveau and J. Katz, 'On the properties of similarity subgrid-scale models as deduced from measurements in a turbulent jet', *J. Fluid Mech.*, **275**, 89–119 (1994).
14. K.B. Shah and J.H. Ferziger, 'A new non-eddy viscosity subgrid-scale model and its application to channel flow', *Annual Research Briefs*, Center for Turbulence Research, 1995, pp. 73–91.
15. D.C. Leslie and G.L. Quarini, 'The application of turbulence theory to the formulation of subgrid modelling procedures', *J. Fluid Mech.*, **91**, 65–91 (1979).
16. U. Piomelli, P. Moin and J.H. Ferziger, 'Model consistency in large-eddy simulation of turbulent channel flows', *Phys. Fluids*, **31**, 1884–1891 (1988).
17. F.M. Najjar and D.K. Tafti, 'Study of discrete test filters and finite difference approximations for the dynamic subgrid-scale stress model', *Phys. Fluids*, **8**, 1076–1088 (1996).
18. K. Jansen, 'Unstructured-grid large-eddy simulation of flow over an airfoil', *Annual Research Briefs*, Center for Turbulence Research, 1994, pp. 161–173.
19. M. Germano, 'Differential filters for the large-eddy numerical simulation of turbulent flows', *Phys. Fluids*, **29**, 1755–1757 (1986).
20. M. Germano, 'Differential filters of elliptic type', *Phys. Fluids*, **29**, 1757–1758 (1986).
21. C.K.N. Tam and J.C. Webb, 'Dispersion-relation-preserving finite difference schemes for computational acoustics', *J. Comput. Phys.*, **107**, 262–281 (1993).
22. E. David, 'Modélisation des écoulements compressibles et hypersoniques: une approche instationnaire', *These de Doctorat*, de l'INPG, Grenoble, France, 1993.

